RSC Advances

RSC Advances

www.rsc.org/advances

ROYAL SOCIETY OF CHEMISTRY

www.rsc.org/advances

ARTICLE TYPE

Large resistive switching in Pt/BNT/HfO$_2$/Pt capacitors

H. J. Song,[a,b] **J. B. Wang,***[a,b] **X. L. Zhong,***[a,b] **J. J. Cheng,**[a,b] **and G. K. Zhong**[a,b]

5 A large resistive switching (RS) of 4 orders is observed in Pt/Bi$_{3.15}$Nd$_{0.85}$Ti$_3$O$_{12}$(BNT)/HfO$_2$/Pt capacitors. The studies of the polarization–voltage loop, capacitance–voltage loop, the fitting current–voltage data, and the current–temperature curves suggest that the RS is mainly induced by the formation/rupture of conductive filament which is induced by inserting the HfO$_2$ dielectric layer in the Pt/BNT/Pt capacitor. The results demonstrate a possibility to control the RS characteristics by modulating the RS mechanism in 10 the polycrystalline ferroelectric thin films.

Introduction

Recently, the resistive switching effect (RS) of high-quality epitaxial[1-6] and polycrystalline[7-17] ferroelectric thin films has been studied extensively because it is possible to achieve great 15 performance of high reliability, high resistive ratio, high speed, high reproducibility, and low write power in memory, memristor,[18] even in neural devices,[19, 20] and so on. Compared with epitaxial films, polycrystalline ferroelectric thin films show advantages in practical use, such as the cheap substrates, the 20 compatibility with the well-established Si technology, and the simple preparing process.[15, 21] However, the RS mechanisms in polycrystalline ferroelectric thin films are various.[11, 14] Generally speaking, the RS in the reported polycrystalline ferroelectric thin films is either modulated by the ferroelectric polarization or 25 mediated by the defects. The RS modulated by the ferroelectric polarization shows high reliability and good uniformity,[16] while the defect mediated one demonstrates a high resistive ratio.[9, 11] Furthermore, these two RS mechanisms are interactional and competitive, and the relation or competition is depended on the 30 effect of the ferroelectric polarization and defects.[14, 15, 17] Thus, the relation or competition of these two RS with different

characteristics provides a possibility to control the RS characteristics by modulating the RS mechanism in the polycrystalline ferroelectric thin films.

35 In our previous work,[22] the RS mainly induced by the ferroelectric polarization modulated switchable diode effect in Bi$_{3.15}$Nd$_{0.85}$Ti$_3$O$_{12}$ (BNT) polycrystalline ferroelectric thin films was found by controlling the oxygen vacancies. In this study, the RS is studied in BNT polycrystalline ferroelectric thin films 40 based capacitors by inserting a HfO$_2$ dielectric layer between the metallic electrode and the polycrystalline BNT thin film in order to highlight the effect of the defect on the RS, since the HfO$_2$ layer could concentrate the electric field at the interface of dielectric/ferroelectric with low/high dielectric constant and 45 decrease the ferroelectric polarization of the BNT above.[23, 24] A large RS of 4 orders is observed, and its physical origin is studied by combining the polarization–voltage loops, the fitting current–voltage data, and the current–temperature curves.

Experimental

50 A 20 nm thick HfO$_2$ layer was deposited on Pt/Ti/SiO$_2$/Si(100) substrate by pulsed laser deposition (PLD) using a KrF excimer
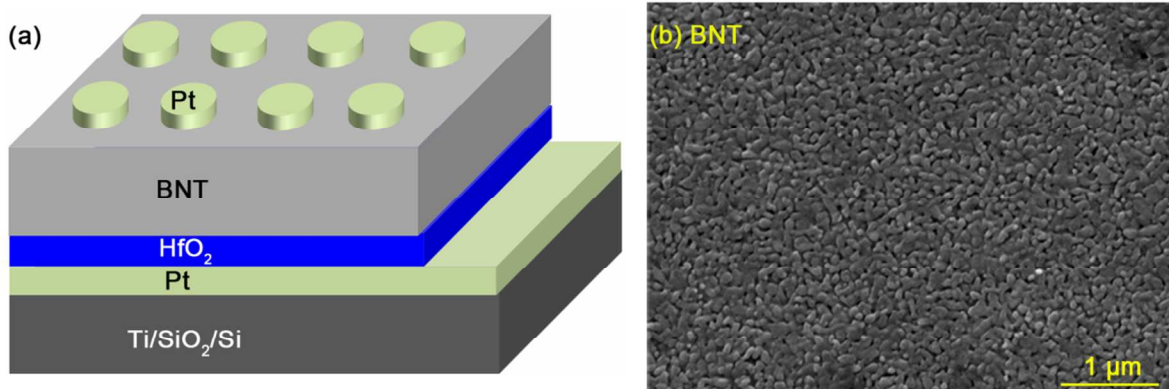

Fig. 1 (a) Schematic illustration of the Pt/BNT/HfO$_2$/Pt capacitors and (b) SEM image of the surface for BNT film
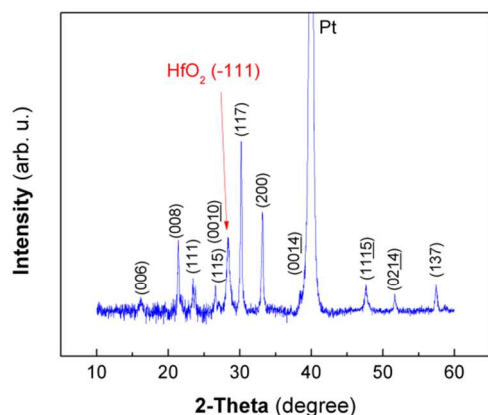
ARTICLE TYPE

Fig. 2 XRD pattern of the BNT/HfO₂ double layers film on the Pt/Ti/SiO₂/Si substrate

laser with a wavelength of 248 nm, followed by annealing for 30 min at 500 °C in air. Then a 220 nm thick BNT polycrystalline thin film was fabricated on the HfO₂ layer using a chemical solution deposition technique annealed layer-by-layer at 720 °C for 20 min in total by a rapid thermal annealing process in air. Finally, Pt dot electrodes with diameter of 100 μm were deposited on the top surface of the BNT film by DC sputtering through a shadow mask to form the Pt/BNT/HfO₂/Pt capacitors. The schematic illustration of the Pt/BNT/HfO₂/Pt capacitors is shown in Fig. 1(a). More details of the fabrication were described in our early works.[22, 25] The morphologies and the structures of the films were characterized by scanning electron microscopy (SEM) and X-ray diffraction (XRD) with Cu K_α radiation. Current–voltage (I–V) curves, capacitance–voltage (C–V) loop, current–time (I–t) curves, and current–temperature (I–T) curves were measured via

an Agilent B1500A semiconductor device analyzer. During the electrical measurements, the bias voltages were applied on the top electrode while the bottom electrode was grounded. Polarization–voltage (P–V) hysteresis loops were measured using a Radiant Technologies Precision Workstation ferroelectric test system, where the drive voltage is applied to the Pt top electrodes.

Results and discussion

The surface morphologies of the BNT film on the HfO₂/Pt/Ti/SiO₂/Si substrate are shown in Fig. 1(b). It can be seen that the surface of the BNT film is relatively rough and the polycrystalline film is composed of dot and columnar grains. Some pores are observed between the crystalline grains. Fig. 2 shows the XRD pattern of the BNT/HfO₂ double layers film on the Pt/Ti/SiO₂/Si substrate. The peaks of Pt electrode, HfO₂ film and BNT film can be seen in the pattern. For the HfO₂ film, there is a (-111) peak of the monoclinic structure. For the BNT film, all the peaks can be indexed according to the standard powder diffraction data of Bi₄Ti₃O₁₂, which indicates that the BNT film is polycrystalline with a single phase of bismuth-layered perovskite structure. Moreover, the (117) and (200) peaks of BNT have a high relatively diffraction intensity because the layer-by-layer annealing process could promote the growth of (117)-oriented and a-axis-oriented grains.[26, 27] The a-axis-oriented and (117)-oriented grains are associated with the dot and columnar grains, which corresponds with the results of SEM images in Fig. 1(b).

Fig. 3(a) shows the I–V curves of the Pt/BNT/Pt capacitor plotted on semi-log scales for the first 20 cycles by sweeping the bias voltage of the Pt top electrode from 0 to 12 V and back to 0 V, then from 0 to −12 V and back to 0 V, repeatedly. The arrows
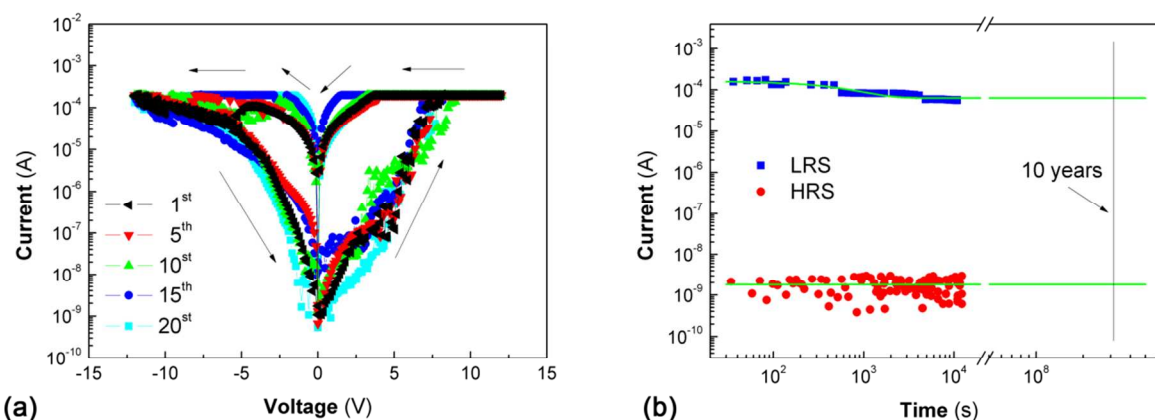
Fig. 3 Resistive switching characteristics of the Pt/BNT/HfO₂/Pt capacitor for (a) the I–V curves with a current compliance of 0.02 mA plotted on semi-log scales for the first 20 cycles by sweeping the bias voltage of the Pt top electrode and (b) the retention capacity of the LRS and HRS. The sweep direction of applied bias voltage is 0→12 V→0→−12 V→0 represented by the arrows. The voltage of SET/RESET operation is +/−12 V and the time is 100 ms, and the voltage for recording the current is 2 V during the retention test.

Journal Name

ARTICLE TYPE

Fig. 4 *P–V* loop at 1 KHz (a) and *C–V* loop at 1 MHz, 800 KHz and 500 KHz (b) of the Pt/BNT/HfO$_2$/Pt capacitor.
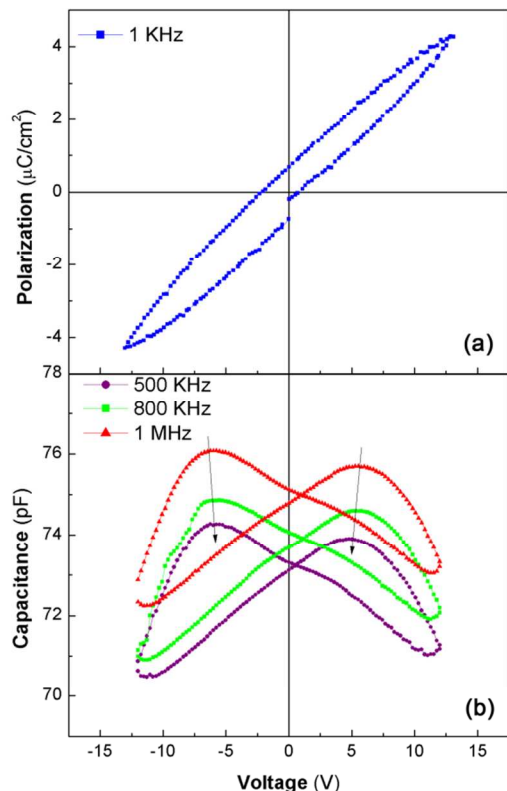
5 are the sweep directions of the applied bias voltage. In order to prevent permanent dielectric breakdown during the cycles, a current compliance of 0.02 mA was fixed. The *I–V* curves in Fig. 3(a) show a distinct hysteresis behavior, indicating a large resistive switching. And the resistive switching is a bipolar-type 10 switching with zero-crossing hysteretic *I–V* characteristics: the SET from the high resistance state (HRS) to the low resistance state (LRS) is at the positive bias region, and the RESET from LRS back to HRS is at the negative bias region. The zero-crossing hysteretic *I–V* characteristics is different from the one 15 induced by a ferroelectric polarization modulated switchable diode effect,[3, 22, 28, 29] where the *I–V* curves show a non-crossing hysteretic characteristics. Moreover, the current ratio of LRS/HRS is more than 4 orders at 2 V, which is larger than that modulated by ferroelectric polarization observed in the epitaxial 20 films or nano-structures, and approaches that in unipolar RS mediated by defects in polycrystalline films.[9, 29] Moreover, the current in LRS is as high as 10^{-4} A. During the growth of BNT polycrystalline ferroelectric thin films, the layer-by-layer annealing process with the high annealing temperature of 720 °C

25 and the long total dwell time of 20 min is used, which will induce a greater deficiency of bismuth in the BNT thin film. For the condition of electrical neutrality, the oxygen vacancy would increase and gather in the grain boundary or domain wall under applied electric field where the free energy is lowest. Thus, the 30 leakage current of the BNT film has been increased.[30-32] Meanwhile, from the Fig. 3(a), it can be seen that the LRS/HRS can be reversed repeatedly without large decay during the first 20 cycles. In detail, it can be seen that the current of LRS at ~2 V is steadier than the one of HRS.

35 In order to verify the potential application for the nonvolatile memory, the current at 2 V for the Pt/BNT/HfO$_2$/Pt capacitor was recorded with time after the SET/RESET operation. The SET/RESET operation is holding the bias of +/−12 V for 100 ms on the top Pt electrodes. For showing the retention capacity more 40 clearly, the dates are extrapolated to 10 years. The results are shown in Fig. 3(b). It can be seen that the current of LRS is stable with a little decrease at about 600–4000 s, while the current of HRS is fluctuant during the test time of 1.3×10^4 s. Nevertheless, the current ratio of LRS/HRS keeps more than 4 orders, which 45 shows a good nonvolatile memory characteristics.

For understanding the effect of the ferroelectric polarization on RS, the *P–V* loop of the Pt/BNT/HfO$_2$/Pt capacitor were measured at a frequency of 1 kHz as shown in Fig. 4(a). It can be seen that the maximum/remnant polarization is about 4.3/0.7 50 μC/cm^2, the coercive voltage is about ±2 V, and the loop is hardly seen and the curve tilts like a paraelectric characteristic, indicating that the polarization of BNT thin film is restrained by inserting the HfO$_2$ layer. The reason is that the thickness ratio of HfO$_2$/BNT in this study is about 0.1 which would cause a large 55 depolarization field,[24] and the voltage drop in the HfO$_2$ layer is large when it connects in series with the BNT ferroelectric film in the Pt/BNT/HfO$_2$/Pt capacitor. For validating the physical origin, *C–V* loop at a high frequency of 1 MHz, 800 KHz and 500 KHz of the Pt/BNT/HfO$_2$/Pt capacitor was tested. During the *C–V* test, 60 a delay time of 200 ms was adopted to ensure a slowly changing bias. The results are shown in Fig. 4(b). A butterfly curve can be seen from the *C–V* curve, indicating the ferroelectricity of the BNT film. The capacitance of the Pt/BNT/HfO$_2$/Pt capacitor is 70–77 pF, which is much lower than that of the Pt/BNT/Pt 65 capacitor.[33] The reason is that the BNT ferroelectric film connects in series with the HfO$_2$ film in the Pt/BNT/HfO$_2$/Pt capacitor. Moreover, the voltage of the maxima for capacitance at 1 MHz is about ±6 V, which is larger than the coercive voltage from *P–V* loop in Fig. 4(a). Meanwhile, it can be seen that the coercive 70 voltage from *C–V* shifts toward low voltage form 1 MHz to 500 KHz. The difference and shift stem from the traps at the electrode interfaces and the interfaces of ferroelectric/dielectric for the interface traps would affect the capacitance via carrier under the voltage bias.[34, 35] Combining the *I–V* curves (Fig. 3(a)) with the 75 *P–V* and *C–V* curves (Fig. 4), it can be found that the RS observed in the Pt/BNT/HfO$_2$/Pt capacitor with the restrained ferroelectric properties is not mainly induced by the ferroelectric
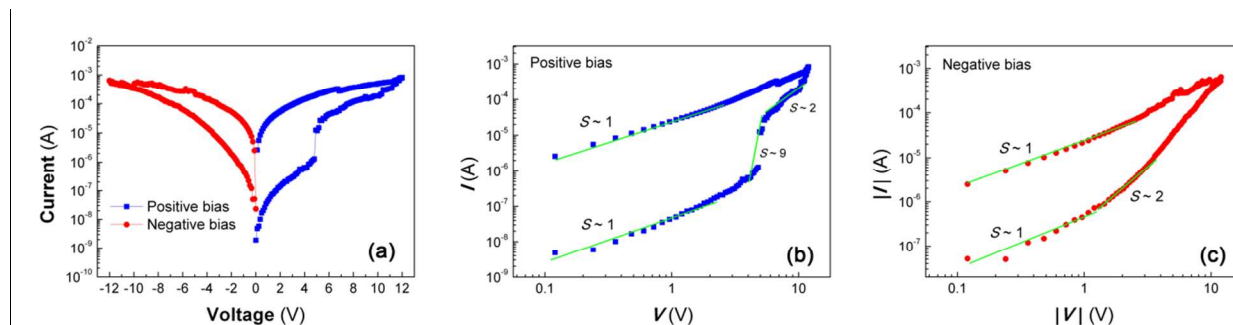
polarization.

Fig. 5 *I–V* curve without current compliance (a) and the logarithm plot of the HRS and LRS at positive (b) and negative bias region (c) of the Pt/BNT/HfO₂/Pt capacitor

To further understand the physical origin of the RS, the *I–V* curve without current compliance and the conduction mechanisms of both LRS and HRS at positive and negative bias region for the Pt/BNT/HfO₂/Pt capacitor were studied by fitting the *I–V* data in several models.[9] The results are shown in Fig. 5. Figs. 5(b) and 5(c) show the best fittings with logarithm plot for positive and negative bias. For the positive bias region (Fig. 5(b)), it can be seen that the curve of HRS at positive bias divides into three parts. The slope (*S*) of the low voltage region is about 1, suggesting an Ohmic behaviour; at the higher voltage, the slope turns to 9; at the further higher voltage, the slope is about 2, suggesting a Child's law region. The results of the slopes for the HRS suggest a space charge limited current (SCLC) conduction. However, it cannot be neglected that the Simmons is a second possible mechanism for observed linear region at low voltage.[36] Similarly, in Fig. 5(c), the Ohmic (*S*~1) and child's law (*S*~2) regions can be seen from the curve of HRS at the negative bias. Moreover, the slope of the LRS at negative bias is about 1. Ohmic and SCLC conductions are bulk-limited mechanism, which further implies that the RS is mainly induced by conductive defects or impurities, but not induced by the ferroelectric polarization. For the RS induced by ferroelectric polarization-modulated interface barriers between the metallic electrodes and the semiconducting ferroelectric, the conduction of HLS and LRS is dominant by interface-limited mechanism,[4, 37, 38] which is different from the bulk-limited mechanism found in Fig. 5. Therefore, it can be deduced that the RS is mainly induced by defects from the conduction mechanisms of both LRS and HRS.

Furthermore, the currents of LRS and HRS for the Pt/BNT/HfO₂/Pt capacitor with temperature ranging from 25 to 175 °C were measured repeatedly as shown in Fig. 6. It can be seen that the current of LRS decreases with the increase of temperature below 125 °C, exhibiting a metallic-like behaviour. This phone phenomenon can also be found in the LRS of HfO₂ in which the RS is associated with the filaments composed of oxygen-vacancy.[39] And the current of LRS suddenly drops at about 125~150 °C. However, the current of HRS is stable and shows little increase in the temperature range from 25 to 175 °C. The temperature dependence of current for the LRS and HRS is fitted by the equation of $I=I_0 \exp(-E_a/\kappa T)$, where κ is the Boltzmann constant and E_a is the thermal activation energy. The ln(*I*)–*T* curve is shown in the insets (a) and (b) of Fig. 6. It can be calculated that the E_a for LRS is negative and the one for HRS is about 94.3 meV. Combining with the results of Fig. 4, the E_a
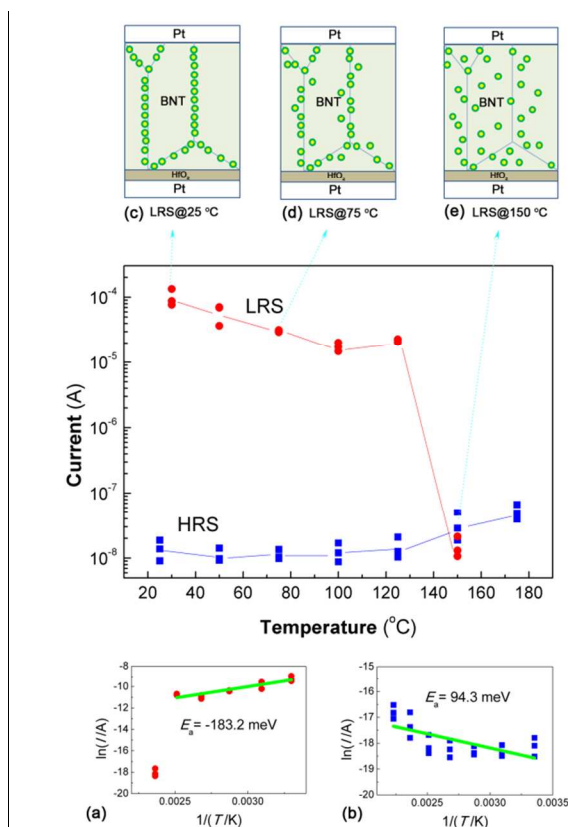

Fig. 6 The temperature dependences of both LRS and HRS for the Pt/BNT/HfO₂/Pt capacitor. The insets (a) and (b) show the Arrhenius plot of the LRS and HRS, the insets (c), (d) and (e) show the schematic diagrams of the distributions for oxygen vacancies of LRS at different temperatures. The oxygen vacancies and grain boundaries are represented by the green circles and the blue solid lines, respectively.

changes from negative values for the LRS state to 94.3 meV for the HRS state is consistent with a conduction change from that controlled by the ohmic filament for LRS to that controlled by the semiconducting interface having local defect states for HRS.[39, 40] However, the value of E_a is low. Thus, the carrier can surmount the barrier easily, so the conduction is still mainly bulk-limited mechanism as shown in Fig. 5. During the growth of the polycrystalline BNT thin film, the oxygen vacancies would be formed as suggested by the large leakage current in Fig. 3 and 5, and they would become highly mobile under high temperature.[11,

[37, 41] The distributions for oxygen vacancies of LRS at different temperatures is sketched in the insets (c), (d) and (e) of Fig. 6. At room temperature (Inset (c) of Fig. 6), the oxygen vacancies of LRS gather at the grain boundaries under a voltage bias and form a conductive filament. With the increase of the temperature (Inset (d) of Fig. 6), some of the oxygen vacancies would move away from the grain boundaries for the thermal stimulation. When the temperature increases above 125 °C (Inset (e) of Fig. 6), the oxygen vacancies of LRS would run away from the grain boundary to get a new equilibrium and its distribution becomes more random like in HRS, so the current of LRS decreases. In all, the results of Fig. 6 imply that the RS is induced by the oxygen vacancies.

As mentioned above, a possible origin for the resistance switching is the oxygen vacancies conductive filament formation/rupture.[8, 42, 43] Under the positive applied electric field, the oxygen vacancies would gather in the grain boundary, and form a conductive filament, so the device switches into the LRS (*i.e.*, SET). Then under the negative applied electric field, some of the oxygen vacancies would recover into the grain interior, and the conductive filament rupture, so the device switching into the HRS (*i.e.*, RESET). Furthermore, the poles in the BNT polycrystalline thin film may give a guide to form the conductive filament, because there is an intensive electric field around the pore.[44] Simultaneously, the relative dielectric constant is low for HfO_2 while high for BNT.[25, 33] When these two layers with low and high dielectric constant respectively combine together, the electric field at their interface would be more concentrated, and the concentrated electric field could improve the RS characteristics induced by a conductive filament.[23]

Conclusions

In conclusion, a large resistive switching (RS) of more than 4 orders is found in Pt/BNT/HfO_2/Pt capacitors. And the resistive switching is a bipolar-type switching with zero-crossing hysteretic *I–V* characteristics. The studies of polarization–voltage loop, capacitance–voltage loop at high frequency, fitting current–voltage data and current–temperature characteristics suggest that the formation/rupture of conductive filament consisting of oxygen vacancies at the grain boundaries of the BNT thin films is the main physical origin of the RS. The HfO_2 dielectric layer promotes the formation of conductive filament by concentrating electric field at the interface of dielectric/ferroelectric and restraining the ferroelectric polarization of the above BNT. The results demonstrate a general paradigm to control the RS characteristics by modulating the RS mechanism in the polycrystalline ferroelectric thin films.

Acknowledgements

Notes and references

[a] School of Materials Science and Engineering, Xiangtan University, Xiangtan 411105, Hunan, China. E-mail: jbwang@xtu.edu.cn; xlzhong@xtu.edu.cn

[b] Key Laboratory of Low Dimensional Materials and Application Technology of Ministry of Education, Xiangtan University, Xiangtan 411105, Hunan, China

1. Z. Wen, C. Li, D. Wu, A. Li and N. Ming, *Nat. Mater.*, 2013, **12**, 617-621.
2. A. Q. Jiang, C. Wang, K. J. Jin, X. B. Liu, J. F. Scott, C. S. Hwang, T. A. Tang, H. B. Lu and G. Z. Yang, *Adv. Mater.*, 2011, **23**, 1277-1281.
3. C. Wang, K.-j. Jin, Z.-t. Xu, L. Wang, C. Ge, H.-b. Lu, H.-z. Guo, M. He and G.-z. Yang, *Appl. Phys. Lett.*, 2011, **98**, 192901.
4. D. Pantel, S. Goetze, D. Hesse and M. Alexe, *ACS Nano*, 2011, **5**, 6032-6038.
5. A. Tsurumaki, H. Yamada and A. Sawa, *Adv. Funct. Mater.*, 2012, **22**, 1040-1047.
6. Y. Park, K. Sung, C. Won, J. Jung and N. Hur, *J. Appl. Phys.*, 2013, **114**, 094101.
7. Z. B. Yan, S. Z. Li, K. F. Wang and J. M. Liu, *Appl. Phys. Lett.*, 2010, **96**, 012103.
8. K. Yin, M. Li, Y. Liu, C. He, F. Zhuge, B. Chen, W. Lu, X. Pan and R.-W. Li, *Appl. Phys. Lett.*, 2010, **97**, 042101.
9. Z. Yan, Y. Guo, G. Zhang and J. M. Liu, *Adv. Mater.*, 2011, **23**, 1351-1355.
10. Y. Shuai, S. Zhou, D. Bürger, M. Helm and H. Schmidt, *J. Appl. Phys.*, 2011, **109**, 124117.
11. L. Liu, S. Zhang, Y. Luo, G. Yuan, J. Liu, J. Yin and Z. Liu, *J. Appl. Phys.*, 2012, **111**, 104103.
12. W. Shen, A. Bell, S. Karimi and I. M. Reaney, *Appl. Phys. Lett.*, 2012, **100**, 133505.
13. J.-J. Huang, T.-C. Chang, C.-C. Yu, H.-C. Huang, Y.-T. Chen, H.-C. Tseng, J.-B. Yang, S. M. Sze, D.-S. Gan, A.-K. Chu, J.-Y. Lin and M.-J. Tsai, *Appl. Phys. Lett.*, 2013, **103**, 042902.
14. X. Tang, X. Zhu, J. Dai, J. Yang, L. Chen and Y. Sun, *J. Appl. Phys.*, 2013, **113**, 043706.
15. M.-X. Zhou, B. Chen, H.-B. Sun, J.-G. Wan, Z.-W. Li, J.-M. Liu, F.-Q. Song and G.-H. Wang, *Nanotechnology*, 2013, **24**, 225702.
16. Y. Yao, B. Zhang, L. Chen, Y. Yang, Z. Wang, H. N. Alshareef and X. X. Zhang, *J. Phys. D: Appl. Phys.*, 2013, **46**, 055304.
17. Y. Guo, B. Guo, W. Dong, H. Li and H. Liu, *Nanotechnology*, 2013, **24**, 275201.
18. A. Chanthbouala, V. Garcia, R. O. Cherifi, K. Bouzehouane, S. Fusil, X. Moya, S. Xavier, H. Yamada, C. Deranlot and N. D. Mathur, *Nat. Mater.*, 2012, **11**, 860-864.
19. S. Li, F. Zeng, C. Chen, H. Liu, G. Tang, S. Gao, C. Song, Y. Lin, F. Pan and D. Guo, *J. Mater. Chem. C*, 2013, **1**, 5292.
20. F. Zeng, S. Li, J. Yang, F. Pan and D. Guo, *RSC Advances*, 2014, **4**, 14822.
21. J. Wu and J. Wang, *Acta Mater.*, 2010, **58**, 1688-1697.
22. H. J. Song, J. B. Wang, X. L. Zhong, J. J. Cheng, L. H. Jia, F. Wang and B. Li, *Appl. Phys. Lett.*, 2013, **103**, 262901.
23. J.-W. Huang, R. Zhang, T.-C. Chang, T.-M. Tsai, K.-C. Chang, J. C. Lou, T.-F. Young, J.-H. Chen, H.-L. Chen, Y.-C. Pan, X. Huang, F. Zhang, Y.-E. Syu and S. M. Sze, *Appl. Phys. Lett.*, 2013, **102**, 203507.
24. A. K. Tagantsev, M. Landivar, E. Colla and N. Setter, *J. Appl. Phys.*, 1995, **78**, 2623.
25. Z. Zhang, X. Zhong, Y. Zhang, J. Wang, C. Lu, W. Ye and Y. Zhou, *EPL (Europhysics Letters)*, 2012, **98**, 27011.
26. Y.-C. Chen, Y.-M. Sun, C. P. Lin and J.-Y. Gan, *J. Cryst. Growth*, 2004, **268**, 210-214.
27. B. Yang, D.-M. Zhang, B. Zhou, L.-H. Huang, C.-D. Zheng, Y.-X. Wu, D.-Y. Guo and J. Yu, *J. Cryst. Growth*, 2008, **310**, 4511-4515.
28. T. Choi, S. Lee, Y. J. Choi, V. Kiryukhin and S. W. Cheong, *Science*, 2009, **324**, 63-66.
29. S. Hong, T. Choi, J. H. Jeon, Y. Kim, H. Lee, H. Y. Joo, I. Hwang, J. S. Kim, S. O. Kang and S. V. Kalinin, *Adv. Mater.*,

2013, **25**, 2339-2343.

30. K.-T. Kim and C.-I. Kim, *Microelectron. Eng.*, 2004, **71**, 266-271.
31. F. Hou, M. Shen and W. Cao, *Thin Solid Films*, 2005, **471**, 35-39.
32. X. J. Zheng, W. M. Yi, Y. Q. Chen, Q. Y. Wu and L. He, *Scr. Mater.*, 2007, **57**, 675-678.
33. X. L. Zhong, J. B. Wang, X. J. Zheng, Y. C. Zhou and G. W. Yang, *Appl. Phys. Lett.*, 2004, **85**, 5661.
34. J. F. Scott, *Ferroelectric memories*, Springer, 2000.
35. C. Brennan, *Integr. Ferroelectr.*, 1995, **9**, 335-346.
36. J. F. Scott, *J. Phys.: Condens. Matter*, 2014, **26**, 142202.
37. D. Lee, S. H. Baek, T. H. Kim, J. G. Yoon, C. M. Folkman, C. B. Eom and T. W. Noh, *Phys. Rev. B*, 2011, **84**, 125305.
38. C. Ge, K.-J. Jin, C. Wang, H.-B. Lu, C. Wang and G.-Z. Yang, *Appl. Phys. Lett.*, 2011, **99**, 063509.
39. L. Goux, Y.-Y. Chen, L. Pantisano, X.-P. Wang, G. Groeseneken, M. Jurczak and D. Wouters, *Electrochem. Solid-State Lett.*, 2010, **13**, G54-G56.
40. S. H. Jeon, B. H. Park, J. Lee, B. Lee and S. Han, *Appl. Phys. Lett.*, 2006, **89**, 042904.
41. C. H. Yang, J. Seidel, S. Kim, P. Rossen, P. Yu, M. Gajek, Y. H. Chu, L. W. Martin, M. Holcomb and Q. He, *Nat. Mater.*, 2009, **8**, 485-493.
42. R. Waser, R. Dittmann, G. Staikov and K. Szot, *Adv. Mater.*, 2009, **21**, 2632-2663.
43. J. J. Yang, D. B. Strukov and D. R. Stewart, *Nat. Nanotechnol.*, 2012, **8**, 13-24.
44. T.-M. Tsai, K.-C. Chang, R. Zhang, T.-C. Chang, J. C. Lou, J.-H. Chen, T.-F. Young, B.-H. Tseng, C.-C. Shih, Y.-C. Pan, M.-C. Chen, J.-H. Pan, Y.-E. Syu and S. M. Sze, *Appl. Phys. Lett.*, 2013, **102**, 253509.